

# Multisecond ligand dissociation dynamics from atomistic simulations

Steffen Wolf,<sup>1,\*</sup> Benjamin Lickert,<sup>1</sup> Simon Bray,<sup>1,2</sup> and Gerhard Stock<sup>1,\*</sup>

<sup>1</sup>*Biomolecular Dynamics, Institute of Physics, Albert Ludwigs University, 79104 Freiburg, Germany*

<sup>2</sup>*Present address: Bioinformatics Group, Department of Computer Science, Albert Ludwigs University, 79110 Freiburg, Germany*

(Dated: 12 June 2020)

Coarse-graining of fully atomistic molecular dynamics simulations is a long-standing goal in order to allow the description of processes occurring on biologically relevant timescales. For example, the prediction of pathways, rates and rate-limiting steps in protein-ligand unbinding is crucial for modern drug discovery. To achieve the enhanced sampling, we first perform dissipation-corrected targeted molecular dynamics simulations, which yield free energy and friction profiles of the molecular process under consideration. In a second step, we use these fields to perform temperature-boosted Langevin simulations which account for the desired molecular kinetics occurring on multisecond timescales and beyond. Adopting the dissociation of solvated sodium chloride as well as trypsin-benzamidine and Hsp90-inhibitor protein-ligand complexes as test problems, we are able to reproduce rates from molecular dynamics simulation and experiments within a factor of 2–20, and dissociation constants within a factor of 1–4. Analysis of the friction profiles reveals that binding and unbinding dynamics are mediated by changes of the surrounding hydration shells in all investigated systems.

Classical molecular dynamics (MD) simulations in principle allow us to describe biomolecular processes in atomistic detail<sup>42</sup>. Prime examples include the study of protein complex formation<sup>2</sup> and protein-ligand binding and unbinding<sup>3,4</sup>, which constitute key steps in biomolecular function. Apart from structural analysis, the prediction of kinetic properties has recently become of interest, since optimized ligand binding and unbinding kinetics have been linked to an improved drug efficacy<sup>5–9</sup>. Since these processes typically occur on timescales from milliseconds to hours, however, they are out of reach for unbiased all-atom MD simulations which currently reach microsecond timescales. To account for rare biomolecular processes, a number of enhanced sampling techniques<sup>10–18</sup> have been proposed. These approaches all entail the application of a bias to the system in order to enforce motion along a usually one-dimensional reaction coordinate  $x$ , such as the protein-ligand distance.

While the majority of the above methods focuses on the calculation of the stationary free energy profile  $\Delta G(x)$ , several approaches have recently been suggested that combine enhanced sampling with a reconstruction of the dynamics of the process<sup>19–21</sup>. In this vein, we recently proposed dissipation-corrected targeted MD (dcTMD), which exerts a pulling force on the system along reaction coordinate  $x$  via a moving distance constraint<sup>10</sup>. By combining a Langevin equation analysis with a cumulant expansion of Jarzynski's equality<sup>23</sup>, dcTMD yields both  $\Delta G(x)$  and the friction field  $\Gamma(x)$ . Reflecting interactions with degrees of freedom orthogonal to those which define the free energy, the friction accounts for the dynamical aspects of the considered process. In this work, we go one step further and use  $\Delta G(x)$  and  $\Gamma(x)$  to run Langevin

simulations, which describe the coarse-grained dynamics along the reaction coordinate and reveal timescales and mechanisms of the considered process. Moreover, we introduce the concept of "temperature boosting" of the Langevin equation, which allows us to speed up the calculations by several orders of magnitude in order to reach biologically relevant timescales.

## THEORY

**Dissipation-corrected targeted molecular dynamics.** To set the stage, we briefly review the working equations of dcTMD derived in Ref. 10. TMD as developed by Schlitter et al.<sup>24</sup> uses a constraint force  $f_c$  that results in a moving distance constraint  $x = x_0 + v_c t$  with a constant velocity  $v_c$ . The main assumption underlying dcTMD is that this nonequilibrium process can be described by a memory-free Langevin equation<sup>42</sup>,

$$m\ddot{x}(t) = -\frac{dG}{dx} - \Gamma(x)\dot{x} + \sqrt{2k_B T \Gamma(x)} \xi(t) + f_c(t), \quad (1)$$

which contains the Newtonian force  $-dG/dx$ , the friction force  $-\Gamma(x)\dot{x}$ , as well as a stochastic force with white noise  $\xi(t)$ , that is assumed to be of zero mean,  $\langle \xi \rangle = 0$ , delta-correlated,  $\langle \xi(t)\xi(t') \rangle = \delta(t-t')$ , and Gaussian distributed. Since the constraint force  $f_c$  imposes a constant velocity on the system ( $\dot{x} = v_c$ ), the total force  $m\ddot{x}$  vanishes. Performing an ensemble average  $\langle \dots \rangle$  of Eq. (1) over many TMD runs, we thus obtain the relation<sup>10</sup>

$$\Delta G(x) = \langle W(x) \rangle - v_c \int_{x_0}^x \Gamma(x') dx'. \quad (2)$$

Here the first term  $\langle W(x) \rangle = \int_{x_0}^x \langle f_c(x') \rangle dx'$  represents the averaged external work performed on the system, and the second term corresponds to the dissipated work

\*<sup>1</sup>email: steffen.wolf@physik.uni-freiburg.de;  
stock@physik.uni-freiburg.de

$W_{\text{diss}}(x)$  of the process expressed in terms of the friction  $\Gamma(x)$ .

While the friction in principle can be calculated in various ways<sup>25,26</sup>, it proves advantageous to invoke Jarzynski's identity<sup>23</sup>,  $e^{-\Delta G(x)/k_{\text{B}}T} = \langle e^{-W(x)/k_{\text{B}}T} \rangle$ , which allows us to calculate  $\Gamma(x)$  directly from TMD simulations. To circumvent convergence problems associated with the above exponential average<sup>27</sup>, we perform a second-order cumulant expansion which gives Eq. (2) with  $W_{\text{diss}}(x) = \langle \delta W^2(x) \rangle / k_{\text{B}}T$ . Expressing work fluctuations  $\delta W$  in terms of the fluctuating force  $\delta f_c$ , we obtain for the friction<sup>10</sup>

$$\Gamma(x) = \frac{1}{k_{\text{B}}T} \int_{t_0}^{t(x)} \langle \delta f_c(t) \delta f_c(t') \rangle dt', \quad (3)$$

which is readily evaluated directly from the TMD simulations.

As discussed in Ref. 10, the derivation of Langevin equation (1) assumes that the pulling speed  $v_c$  is slow compared to the timescale of the bath fluctuations, such that the effect of  $f_c$  can be considered as a slow adiabatic change<sup>28</sup>. This means that the free energy (2) and the friction (3) determined by the nonequilibrium TMD simulations correspond to their equilibrium results. As a consequence, we can use  $\Delta G(x)$  and  $\Gamma(x)$  to describe the unbiased motion of the system via Langevin equation (1) for  $f_c = 0$ . Numerical propagation of the unbiased Langevin equation then accounts for the coarse grained dynamics of the system. In this way, calculations of  $\Delta G(x)$  and  $\Gamma(x)$  as well as dynamical calculations are based on the same theoretical footing (i.e., the Langevin equation), and are therefore expected to yield a consistent estimation of the timescales of the considered process. Moreover, the exact solution of the Langevin equation allows us to directly use the computed fields  $\Delta G(x)$  and  $\Gamma(x)$  and thus to avoid further approximations<sup>29</sup>.

The theory developed above rests on two main assumptions. For one, we have assumed that the Langevin equation (1) provides an appropriate description of nonequilibrium TMD simulations, and applies as well to the unbiased motion ( $f_c = 0$ ) of the system. This means that, due to a timescale separation of slow pulling speed and fast bath fluctuations, the constraint force  $f_c$  enters this equation merely as an additive term. Secondly, to ensure rapid convergence of the Jarzynski equation, we have invoked a cumulant expansion to derive the friction coefficient in Eq. (3), which is valid under the assumption that the distribution of the work is Gaussian within the ensemble. While this assumption may break down if the system of interest follows multiple reaction paths, we have recently shown that we can systematically perform a separation of dcTMD trajectories according to pathways by a nonequilibrium principal component analysis of protein-ligand contacts<sup>37</sup>. This approach bears similarities with the work of Tiwary et al. for the construction of path collective variables<sup>31</sup>. Alternatively, path separation can be based on geometric distances between individual trajectories, making use of the NeighborNet

algorithm<sup>40</sup>. Details on the convergence of the free energy and friction estimates, the path separation, and the choice of the pulling velocity are given in Supplementary Methods and in Supplementary Figs. 1 to 4.

***T*-boosting.** The speed-up of Langevin equation (1) compared to an unbiased all-atom MD simulation is due to the drastic coarse graining of the Langevin model (one instead of  $3N$  degrees of freedom,  $N$  being the number of all atoms). Since the numerical integration of the Langevin equation typically requires a time step of a few femtoseconds (see Supplementary Table 1), however, we still need to propagate Eq. (1) for  $\gtrsim 100 \cdot 10^{15}$  steps to sufficiently sample a process occurring on a timescale of seconds, which is prohibitive for standard computing resources.

As a further way to speed up calculations, we note that the temperature  $T$  enters Eq. (1) via the stochastic force, indicating that temperature is the driving force of the Langevin dynamics. That is, when we consider a process described by a transition rate  $k$  and increase the temperature from  $T_1$  to  $T_2$ , the corresponding rates  $k_1$  and  $k_2$  are related by the Kramers-type expression<sup>29</sup>

$$k_2 = k_1 e^{-\Delta G^\ddagger(\beta_2 - \beta_1)}, \quad (4)$$

where  $\Delta G^\ddagger$  denotes the transition state energy and  $\beta_i = 1/k_{\text{B}}T_i$  is the inverse temperature. Hence, by increasing the temperature we also increase the number  $n$  of observed transition events according to  $n_2/n_1 = k_2/k_1$ .

To exploit this relationship for dcTMD, we proceed as follows. First we employ dcTMD to calculate the Langevin fields  $\Delta G(x)$  and  $\Gamma(x)$  at a temperature of interest  $T_1$ . Using these fields, we then run a Langevin simulation at some higher temperature  $T_2$ , which results in an increased transition rate  $k_2$  and number of events  $n_2$ . In particular, we choose a temperature high enough to sample a sufficient number of events ( $N \gtrsim 100$ ) for some given simulation length. In the final step, we use Eq. (4) to calculate the transition rate  $k_1$  at the desired temperature  $T_1$ .

As Eq. (4) arises as a consequence<sup>29</sup> of Langevin equation (1), the above described procedure, henceforth termed "*T*-boosting," involves no further approximations. It exploits the fact that we calculate fields  $\Delta G(x)$  and  $\Gamma(x)$  at the same temperature for which we eventually want to calculate the rate. We wish to stress that this virtue represents a crucial difference to temperature accelerated MD.<sup>34</sup> In the latter method the free energy  $\Delta G(x)$  is first calculated at a high temperature and subsequently rescaled to a desired low temperature, whereupon  $\Delta G(x)$  in general does change. *T*-boosting avoids this, because by using dcTMD we calculate  $\Delta G(x)$  right away at the desired temperature. We note in passing that a Langevin simulation run at  $T_2$  using fields obtained at  $T_1$  in general does not reflect the coarse-grained dynamics of an MD simulation run at  $T_2$ , but can only be used to recover  $k_1$  from  $k_2$ .

In practice, we perform *T*-boosting calculations at several temperatures  $T_2$  in increments of 25 K to 50 K and

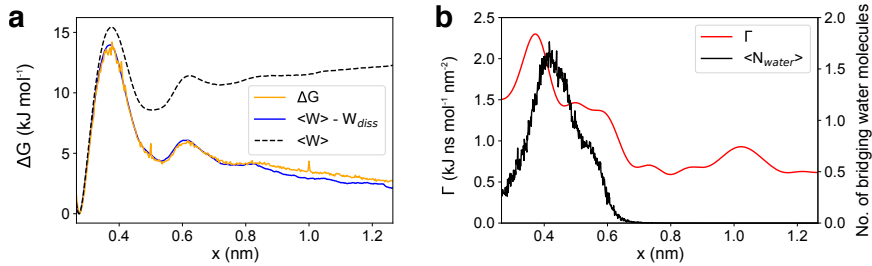


FIG. 1. Dissociation of NaCl in water. (a) Free energy profiles  $\Delta G(x)$  along the interionic distance  $x$ , obtained from a 1  $\mu\text{s}$  long unbiased MD trajectory at 293 K (orange line) and  $1000 \times 1$  ns TMD runs (blue line). Error bars are given in Supplementary Fig. 2. Also shown is the average work  $\langle W(x) \rangle$  calculated from the TMD simulations (dashed black line). (b) Friction profile  $\Gamma(x)$  (red) obtained from dcTMD after Gaussian smoothing together with the average number of water molecules (black), that connect the  $\text{Na}^+$  and  $\text{Cl}^-$  ions in a common hydration shell<sup>33</sup>.

choose the smallest  $T_2$  such that  $N \gtrsim 100$  transitions occur. In the Supporting Information we derive an analytic expression of the extrapolation error as a function of boosting temperatures and achieved number of transitions, from which the necessary length of the individual Langevin simulations can be estimated, in order to achieve a desired extrapolation error. One-dimensional Langevin simulations require little computational effort (1 ms of simulation time at a 5 fs time step take  $\sim 6$  hours of wall-clock time on a single CPU) and are trivial to parallelize in the form of independent short runs. Hence the extrapolation error due to boosting can easily be pushed below 10% and is thus negligible in comparison to systematic errors coming from the dcTMD field estimates.

As shown in Supplementary Table 1, a further increase in efficiency can be achieved if the considered dynamics is overdamped, which is the case for both protein-ligand systems. Since overdamped dynamics neglects the inertia term  $m\ddot{x}$  and therefore does not depend on the mass  $m$ , we may artificially enhance the mass in the Langevin simulations. For the protein-ligand systems, this allows us to increase the integration time step from 1 to 10 fs, i.e., a speed-up of an order of magnitude.

## RESULTS AND DISCUSSION

**Ion dissociation of NaCl in water.** To illustrate the above developed theoretical concepts and test the validity of the underlying approximations, we first consider sodium chloride in water as a simple yet nontrivial model system. For this system, detailed dcTMD as well as long unbiased MD simulations are available<sup>10</sup>, making it a suitable benchmark system for our approach.

Fig. 1a shows the free energy profiles  $\Delta G(x)$  along the interionic distance  $x$ , whose first maximum at  $x \approx 0.4$  nm corresponds to the binding-unbinding transition of the two ions. The second smaller maximum at  $x \approx 0.6$  nm reflects the transition from a common to two separate hydration shells<sup>33</sup>. We find that results for  $\Delta G(x)$  ob-

tained from a 1  $\mu\text{s}$  long unbiased MD trajectory and from dcTMD simulations ( $1000 \times 1$  ns runs with  $v_c = 1$  m/s) match perfectly. Since the average work  $\langle W(x) \rangle$  of the nonequilibrium simulations is seen to significantly overestimate the free energy at large distances, the dissipation correction  $W_{\text{diss}}$  in Eq. (2) is obviously of importance. Figure 1b shows the underlying friction profile  $\Gamma(x)$  obtained from dcTMD, which in part deviates from the lineshape of the free energy. While we also find a maximum at  $x \approx 0.4$  nm, the behavior of  $\Gamma(x)$  is remarkably different for larger distances  $0.5 \lesssim x \lesssim 0.7$  nm, where a region of elevated friction can be found before dropping to lower values. Interestingly, these features of  $\Gamma(x)$  match well the changes of the average number of water molecules bridging both ions<sup>33</sup>. This indicates that the increased friction in Eq. (3) is mainly caused by force fluctuations associated with the build-up of a hydration shell<sup>10</sup>. For  $x \gtrsim 0.8$  nm, the friction is constant within our signal-to-noise resolution.

The dynamics of ion dissociation and association can be described by their mean waiting times and corresponding rates shown in Figure 2a. For the chosen force field, ion concentration and resulting effective simulation box size, the unbiased MD simulation at 293 K yields mean dissociation and association times of  $\tau_D = 1/k_D = 120$  ps and  $\tau_A = 1/(k_A C) = 850$  ps, respectively, where  $C$  denotes a reference concentration (see the Supplementary Methods for details). Using fields  $\Delta G(x)$  and  $\Gamma(x)$  obtained from TMD, the numerical integration of Langevin equation (1) for 1  $\mu\text{s}$  results in  $\tau_D = 420$  ps and  $\tau_A = 3040$  ps. While the dissociation constants  $K_D = k_D/k_A = 1.5$  M from Langevin and MD simulations match perfectly, we find that the Langevin predictions overestimate the correct rates by a factor of  $\sim 3.4$ . The latter may be caused by various issues. For one, to be of practical use, the Langevin model was deliberately kept quite simple. For example, it does not include an explicit solvent coordinate<sup>33,38</sup>, but accounts for the complex dynamics of the solvent merely through the friction field  $\Gamma(x)$ . Moreover, we note that the calculation of  $\Gamma(x)$  via Eq. (3) uses constraints, which have

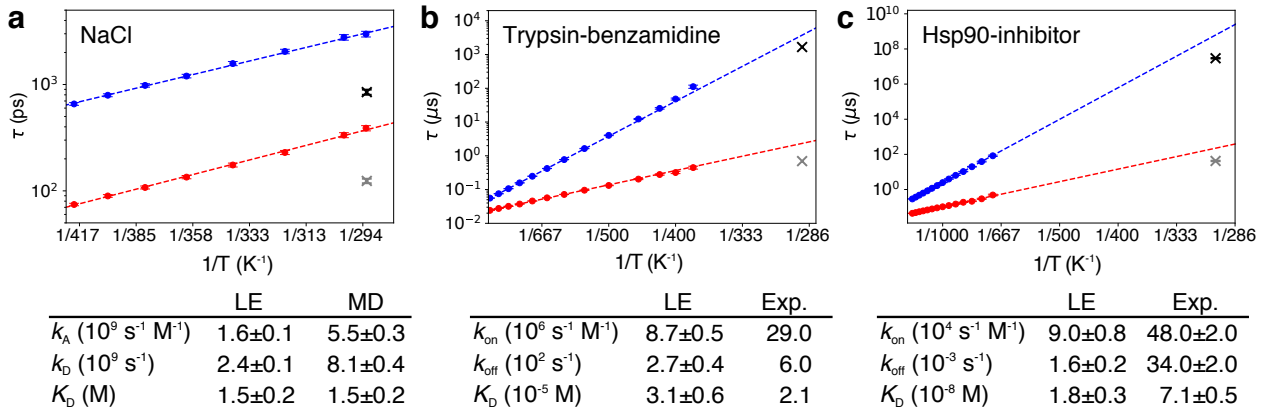


FIG. 2. Mean binding (red) and unbinding (blue) times, drawn as a function of the inverse temperature, obtained from  $T$ -boosted Langevin simulations of (a) solvated NaCl, (b) the trypsin-benzamidine complex and (c) the Hsp90-inhibitor complex. Dashed lines represent fits ( $R^2 = 0.90 - 0.99$ ) to Eq. (4), crosses (binding in grey, unbinding in black) indicate reference results from a unbiased MD simulation<sup>10</sup> and b, c experiment<sup>20,35</sup>. Bars represent the standard error of the mean. Tables below comprise corresponding rates (with  $M$  being the molarity, i.e., mol/l) and reference values. Rate constants were fitted according to Eq. (4) at 290 K and 300 K, respectively, with fit errors as indicated<sup>46</sup>. Dissociation constants were calculated from rate constants.

the effect of increasing the effective friction<sup>45</sup>. This finding is supported by calculations using the data-driven Langevin approach<sup>40,44</sup>, which estimates friction coefficients based on unbiased MD simulations that are consistently smaller than the ones obtained from dcTMD (Supplementary Fig. 5). Considering the simplicity of the Langevin model and the approximate calculation of the friction coefficient by dcTMD, overall we are content with a factor  $\sim 3$  deviation of the predicted kinetics.

To illustrate the validity of the  $T$ -boosting approach suggested above, we performed a series of Langevin simulations for eight temperatures ranging from 290 to 420 K and plotted the resulting dissociation and association times as a function of the inverse temperature (Fig. 2a). Checking the consistency of our approach, a fit to Eq. (4) yields transition state free energies  $\Delta G^\ddagger$  of 13 kJ/mol and 12 kJ/mol for ion dissociation and association, respectively, which agree well with barrier heights of the free energy profile in Fig. 1a. Moreover, dissociation and association times obtained from the extrapolated  $T$ -boosted Langevin simulations ( $\tau_D = 370$  ps,  $\tau_A = 3050$  ps) agree excellently with the directly calculated values. This indicates that high-temperature Langevin simulations can indeed be extrapolated to obtain low-temperature transition rates.

**Trypsin-benzamidine.** Let us now consider the prediction of free energies, friction profiles and kinetics in protein-ligand systems. The first system we focus on is the inhibitor benzamidine bound to trypsin<sup>19,20,43</sup>, which represents a well-established model problem to test enhanced sampling techniques<sup>21,31,44-47</sup>. The slowest dynamics in this system is found in the unbinding process, which occurs on a scale of milliseconds<sup>20</sup>. To capture the kinetics of the unbinding process, so far Markov state models<sup>44,45</sup>, metadynamics<sup>31</sup>, Brownian dynamics<sup>46</sup> and adaptive enhanced sampling methods<sup>21,47</sup> have been em-

ployed.

Here we combined dcTMD simulations and a subsequent nonequilibrium principal component analysis<sup>37</sup> to identify the dominant dissociation pathways of ligands during unbinding from their host proteins (see Supplementary Methods). Figure 3 shows TMD snapshots of the structural evolution along this pathway, its free energy profile  $\Delta G(x)$ , and the associated friction  $\Gamma(x)$ . Starting from the bound state ( $x_1 = 0$  nm),  $\Delta G(x)$  exhibits a single maximum at  $x_2 \approx 0.46$  nm, before it reaches the dissociated state for  $x \gtrsim x_4 = 0.75$  nm. In line with the findings of Tiwary et al.<sup>31</sup>, the maximum of  $\Delta G(x)$  reflects the rupture of the Asp189-benzamidine salt bridge, which represents the most important contact of the bound ligand. Following right after, the friction profile  $\Gamma(x)$  reaches its maximum at  $x_3 \approx 0.54$  nm, where the charged side chain of benzamidine becomes hydrated with water molecules. Similarly to NaCl, the friction peak coincides with the increase in the average number of hydrogen bonds between benzamidine and bulk water. The peak in friction is slightly shifted to higher  $x$ , because the ligand acts as a "plug" for the binding site, and first needs to be (at least partially) removed in order to allow water flowing in. As for the dissociation of NaCl in water, enhanced friction during unbinding appears to be directly linked to a rearrangement of the protein-ligand hydration shell, which is in agreement with recent results from neutron crystallography<sup>43</sup>.

To calculate rates  $k_{\text{on}}$  and  $k_{\text{off}}$  describing the binding and unbinding of benzamidine from trypsin, we performed 10 ms long Langevin simulations along the dominant pathways at thirteen temperatures ranging from 380–900 K. As shown in Fig. 2b, the resulting rates are well fitted ( $R^2 \geq 0.90$ ) by the  $T$ -boosting expression in Eq. (4). Representing the resulting number of transitions as a function of the inverse temperature, we find that at

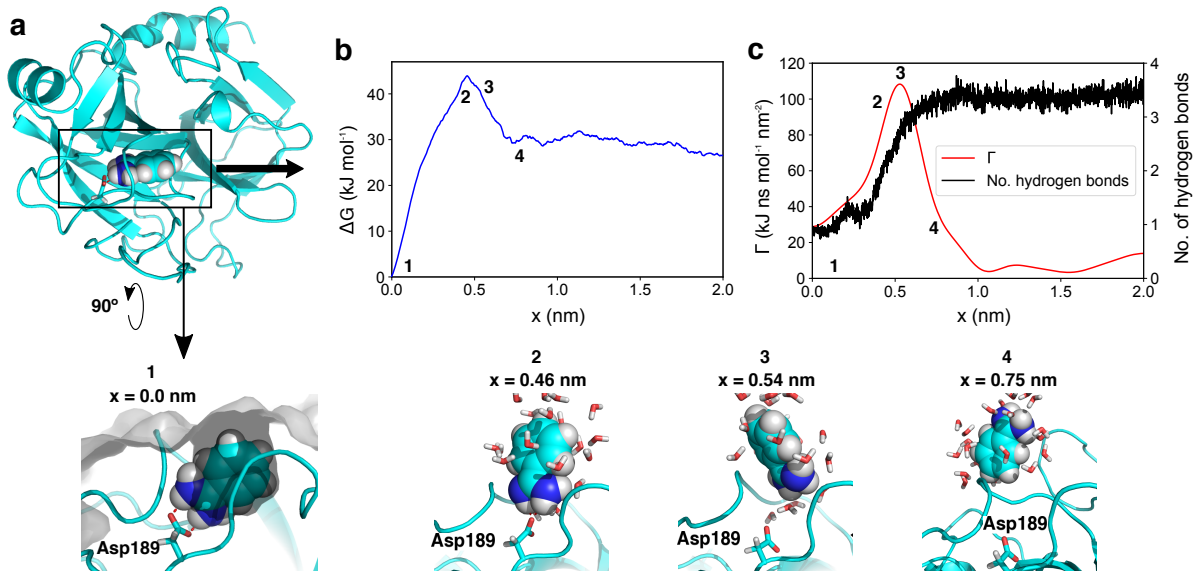


FIG. 3. Unbinding of benzamidine from trypsin. (a) TMD snapshots of the structural evolution in trypsin along the dominant dissociation pathway, showing protein surface in gray, benzamidine as van der Waals spheres, Asp189 and water molecules as sticks. Benzamidine is bound to the protein in a cleft of the protein surface via a bidental salt bridge to Asp189. dcTMD calculations of (b) free energy  $\Delta G(x)$  and (c) (Gaussian smoothed) friction  $\Gamma(x)$  together with the mean number of hydrogen bonds between benzamidine and water. Highlighted are the bound state **1**, transition state **2**, the state with maximal friction **3** and the unbound state **4**. Error bars of free energy and friction estimates are given in Supplementary Fig. 2.

380 K only  $\sim 9$  events happen during a millisecond. That is, to obtain statistically converged rates at 290 K would require Langevin simulations at 290 K on a timescale of seconds. Using temperature boosting with Eq. (4), on the other hand, our high-temperature millisecond Langevin simulations readily yield converged transition rates at 290 K (see Fig. 2b), that is,  $k_{\text{on}} = 8.7 \cdot 10^6 \text{ s}^{-1}\text{M}^{-1}$  and  $k_{\text{off}} = 2.7 \cdot 10^2 \text{ s}^{-1}$ , which underestimate the experimental values<sup>20</sup>  $k_{\text{on}} = 2.9 \cdot 10^7 \text{ s}^{-1}\text{M}^{-1}$  and  $k_{\text{off}} = 6.0 \cdot 10^2 \text{ s}^{-1}$  by a factor of 2–3. Similarly, the calculated  $K_D$  overestimates the experimental result<sup>20</sup> of  $K_D = 2.1 \cdot 10^{-5} \text{ M}$  by a factor of  $\sim 1.5$ . As indicated by a recent review<sup>3</sup> comparing numerous computational methods to calculate (un)binding rates of trypsin-benzamidine, our approach compares quite favorably regarding accuracy and computational effort.

As the extrapolation error due to  $T$ -boosting is negligible (see Supplementary Methods), the observed error is mainly caused by the approximate calculation of free energy and friction fields by dcTMD. In the case of NaCl, we have shown that reliable estimates of the fields (with errors  $\lesssim 1 k_B T$ ) require an ensemble of at least 500 simulations (see Ref. 10 and Supplementary Fig. 2), although the means of  $\Delta G$  and  $\Gamma$  appear to converge already for  $\sim 100$  trajectories. In a similar vein, by performing a Jackknife “leave-one-out” analysis<sup>33</sup>, for trypsin-benzamidine we obtain an error of  $\sim 2 k_B T$  for 150 trajectories (Supplementary Fig. 2). Interestingly, the error of the main free energy barrier is typically comparatively small, because the friction and thus variance of  $W$  increase directly after the barrier. As a consequence,

the sampling error of  $k_{\text{off}}$  is small compared to that of  $k_{\text{on}}$  and the binding free energy. We note that if the experimental binding affinity  $K_D$  is known, it can be used as a further constraint on the error of the free energy and friction fields.

**Hsp90-inhibitor.** The second investigated protein complex is the N-terminal domain of heat shock protein 90 (Hsp90) bound to a resorcinol scaffold-based inhibitor (**1j** in Ref. 21). This protein has recently been established as a test system for investigating the molecular effects influencing binding kinetics<sup>21,35,50,51</sup>, and the selected inhibitor unbinds on a scale of half a minute. From the overall appearance of free energy and friction profiles (Fig. 4), we observe clear similarities to the case of trypsin-benzamidine. That is, the main transition barrier is also found at  $x_2 \approx 0.5$  nm, which stems from the ligand pushing between two helices at this point in order to escape the binding site. Moreover, the friction peaks at  $x_2 \approx 0.5$  nm, as well, but with an additional shoulder at  $x_3 \approx 0.8$  nm, which again coincides with changes of the ligand’s hydration shell. The unbound state is reached after  $x \gtrsim 1.0$  nm. We note that the ligand is again bound to the protein via a hydrogen bond to an aspartate (Asp93) and at a position that is open to the bulk water.

To calculate rates  $k_{\text{on}}$  and  $k_{\text{off}}$ , we again performed 5 ms long Langevin simulations along the dissociation pathway at fourteen different temperatures ranging from 700–1350 K. Rate prediction yields  $k_{\text{on}} = 9.0 \cdot 10^4 \text{ s}^{-1}\text{M}^{-1}$  and  $k_{\text{off}} = 1.6 \cdot 10^{-3} \text{ s}^{-1}$ , and underestimates the experimental<sup>35</sup> values  $k_{\text{on}} = 4.8 \pm 0.2 \cdot 10^5 \text{ s}^{-1}\text{M}^{-1}$  and

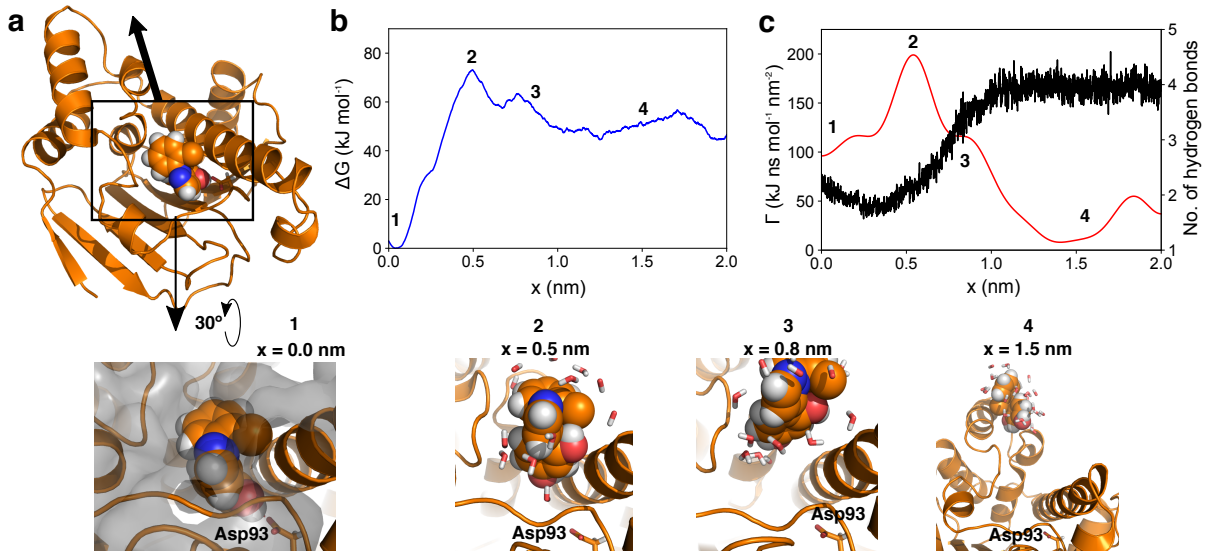


FIG. 4. Unbinding of an inhibitor from the N-terminal domain of Hsp90. (a) Structural evolution along the dissociation pathway in Hsp90, showing protein surface in gray, inhibitor as van der Waals spheres, Asp93 and water molecules as sticks. The inhibitor is bound to the protein in a cleft of the protein surface via a hydrogen bond to Asp93. dcTMD calculations of (b) free energy  $\Delta G(x)$  and (c) (Gaussian-smoothed) friction  $\Gamma(x)$  together with the mean number of hydrogen bonds between inhibitor and water. Highlighted are the bound state **1**, transition state and state with maximal friction **2**, an additional state with increased friction **3** and the unbound state **4**. Error bars of free energy and friction estimates are given in Supplementary Fig. 2. Fluctuations of  $\Gamma(x)$  for  $x \gtrsim 1$  nm are due to noise. Color code as in Fig. 3.

$k_{\text{off}} = 3.4 \pm 0.2 \cdot 10^{-2} \text{ s}^{-1}$  by a factor of 5–20. The resulting value for  $K_D = 1.8 \cdot 10^{-8} \text{ M}$  underestimates the experimental value<sup>35</sup>  $7.1 \cdot 10^{-8} \text{ M}$  by a factor of  $\sim 4$ . Considering that we attempt to predict unbinding times on a time scale of half a minute from sub- $\mu\text{s}$  MD simulations, and that a factor 20 corresponds to a free energy difference of about  $3 k_B T$  (i.e., 15 % of the barrier height in Hsp90), we find this agreement remarkable for a first principles approach which implies many uncertainties of the physical model<sup>52</sup>. We attribute the larger deviation in comparison to trypsin to issues with the sampling of the correct unbinding pathways: especially unbinding rates in the range of minutes to hours fall into the same timescale as slow conformational dynamics of host proteins<sup>35</sup>, requiring a sufficient sampling of the conformational space of the protein as a prerequisite for dcTMD pulling simulations.

## CONCLUSIONS

Using free energy and friction profiles obtained from dcTMD, we have shown that  $T$ -boosted Langevin simulations yield binding and unbinding rates which are well comparable to results from atomistic equilibrium MD and experiments. That is, rates are underestimated by an order of magnitude or less which, in comparison to other methods that have been applied to the trypsin-benzamidine and Hsp90 complexes (see Refs. 3 and 53 for recent reviews), is within the top accuracy currently

achievable. At the same time, the few other methods that aim at predicting absolute rates (such as Markov state models<sup>44,45</sup> and infrequent metadynamics<sup>31,54</sup>) require substantial more MD simulation time, while dcTMD only requires sub- $\mu\text{s}$  MD runs, that is, at least an order of magnitude less computational time. As the extrapolation error due to  $T$ -boosting is negligible, the error is mainly caused by the approximate calculation of free energy and friction fields by dcTMD. We have shown that friction profiles, which correspond to the dynamical aspect of ligand binding and unbinding, may yield additional insight into molecular mechanisms of unbinding processes, which are not reflected in the free energies. Although the three investigated molecular systems differ significantly, in all cases friction was found to be governed by the dynamics of solvation shells.

## METHODS

**MD simulations.** All simulations employed Gromacs v2018 (Ref. 4) in a CPU/GPU hybrid implementation, using the Amber99SB\* force field<sup>1,2</sup> and the TIP3P water model<sup>3</sup>. For each system,  $10^2$ - $10^3$  dcTMD calculations<sup>10</sup> at pulling velocity  $v_c = 1 \text{ m/s}$  were performed to calculate free energy  $\Delta G(x)$  and friction  $\Gamma(x)$ . For the NaCl-water system, dcTMD as well as unbiased MD simulations were taken from Ref. 10. Trypsin-benzamidine complex simulations are based on the 1.7 Å X-ray crystal structure with PDB ID 3PTB (Ref. 19). Simulation

systems of the Hsp90-inhibitor complex were taken from Ref. 21. Detailed information on system preparation, ligand parameterization, MD simulations and pathway separation can be found in the Supplementary Information.

**Langevin simulations.** Langevin simulations employed the integration scheme by Bussi and Parrinello<sup>59</sup>. Details on the performance of this method with respect to the employed integration time step and system mass can be found in the Supplementary Information.

### Data availability

Python scripts for dcTMD calculations, the fastpca program package for nonequilibrium principal component analysis, the data-driven Langevin package, the Langevin simulation code, and Jupyter notebooks for *T*-boosting analysis and sampling error estimation in Langevin simulations are available at our website [www.moldyn.uni-freiburg.de](http://www.moldyn.uni-freiburg.de). Further data is available from the authors upon request.

### REFERENCES

- Berendsen, H. J. C. *Simulating the Physical World* (Cambridge University Press, Cambridge, 2007).
- Pan, A. C. *et al.* Atomic-level characterization of protein–protein association. *Proc. Natl. Acad. Sci. USA* **116**, 4244–4249 (2019).
- Bruce, N. J., Ganotra, G. K., Kokh, D. B., Sadiq, S. K. & Wade, R. C. New approaches for computing ligand–receptor binding kinetics. *Curr. Opin. Struct. Biol.* **49**, 1–10 (2018).
- Rico, F., Russek, A., González, L., Grubmüller, H. & Scheuring, S. Heterogeneous and rate-dependent streptavidin–biotin unbinding revealed by high-speed force spectroscopy and atomistic simulations. *Proc. Natl. Acad. Sci. USA* **116**, 6594–6601 (2019).
- Copeland, R. A., Pompliano, D. L. & Meek, T. D. Drug–target residence time and its implications for lead optimization. *Nat. Rev. Drug Discov.* **5**, 730–739 (2006).
- Swinney, D. C. Applications of Binding Kinetics to Drug Discovery. *Pharmaceut. Med.* **22**, 23–34 (2012).
- Pan, A. C., Borhani, D. W., Dror, R. O. & Shaw, D. E. Molecular determinants of drug–receptor binding kinetics. *Drug Discov. Today* **18**, 667–673 (2013).
- Klebe, G. The Use of Thermodynamic and Kinetic Data in Drug Discovery: Decisive Insight or Increasing the Puzzlement? *ChemMedChem* **10**, 229–231 (2014).
- Copeland, R. A. The drug–target residence time model: a 10-year retrospective. *Nat. Rev. Drug Discov.* **15**, 87–95 (2016).
- Chipot, C. & Pohorille, A. *Free Energy Calculations* (Springer, Berlin, 2007).
- Christ, C. D., Mark, A. E. & van Gunsteren, W. F. Basic Ingredients of Free Energy Calculations: A Review. *J. Comput. Chem.* **31**, 1569–1582 (2010).
- Mitsutake, A., Sugita, Y. & Okamoto, Y. Generalized-ensemble algorithms for molecular simulations of biopolymers. *Biopolymers* **60**, 96 (2001).
- Torrie, G. M. & Valleau, J. P. Non-physical sampling distributions in Monte-Carlo free-energy estimation - umbrella sampling. *J. Comput. Phys.* **23**, 187 – 199 (1977).
- Israelowitz, B., Gao, M. & Schulten, K. Steered molecular dynamics and mechanical functions of proteins. *Curr. Opin. Struct. Biol.* **11**, 224–230 (2001).
- Sprik, M. & Ciccotti, G. Free energy from constrained molecular dynamics. *J. Chem. Phys.* **109**, 7737–7744 (1998).
- Grubmüller, H. Predicting slow structural transitions in macromolecular systems: Conformational flooding. *Phys. Rev. E* **52**, 2893–2906 (1995).
- Barducci, A., Bonomi, M. & Parrinello, M. Metadynamics. *Comput. Mol. Sci.* **1**, 826–843 (2011).
- Comer, J. *et al.* The adaptive biasing force method: everything you always wanted to know but were afraid to ask. *J. Phys. Chem. B* **119**, 1129–1151 (2015).
- Tiwary, P. & Parrinello, M. From metadynamics to dynamics. *Phys. Rev. Lett.* **111**, 230602 (2013).
- Wu, H., Paul, F., Wehmeyer, C. & Noé, F. Multiensemble Markov models of molecular thermodynamics and kinetics. *Proc. Natl. Acad. Sci. USA* **113**, E3221–E3230 (2016).
- Teo, I., Mayne, C. G., Schulten, K. & Lelievre, T. Adaptive Multilevel Splitting Method for Molecular Dynamics Calculation of Benzamidine-Trypsin Dissociation Time. *J. Chem. Theory Comput.* **12**, 2983–2989 (2016).
- Wolf, S. & Stock, G. Targeted molecular dynamics calculations of free energy profiles using a nonequilibrium friction correction. *J. Chem. Theory Comput.* **14**, 6175–6182 (2018).
- Jarzynski, C. Nonequilibrium equality for free energy differences. *Phys. Rev. Lett.* **78**, 2690–2693 (1997).
- Schlitter, J., Engels, M. & Krüger, P. Targeted molecular dynamics - a new approach for searching pathways of conformational transitions. *J. Mol. Graph.* **12**, 84–89 (1994).
- Straub, J. E., Borkovec, M. & Berne, B. J. Calculation of dynamic friction on intramolecular degrees of freedom. *J. Phys. Chem.* **91**, 4995 – 4998 (1987).
- Hummer, G. Position-dependent diffusion coefficients and free energies from Bayesian analysis of equilibrium and replica molecular dynamics simulations. *New J. Phys.* **7**, 34 (2005).
- Vaikuntanathan, S. & Jarzynski, C. Escorted free energy simulations: Improving convergence by reducing dissipation. *Phys. Rev. Lett.* **100**, 190601 (2008).
- Servantie, J. & Gaspard, P. Methods of calculation of a friction coefficient: application to nanotubes. *Phys. Rev. Lett.* **91**, 185503 (2003).
- Hänggi, P., Talkner, P. & Borkovec, M. Reaction-rate theory: fifty years after Kramers. *Rev. Mod. Phys.* **62**, 251 (1990).
- Post, M., Wolf, S. & Stock, G. Principal component analysis of nonequilibrium molecular dynamics simulations. *J. Chem. Phys.* **150**, 204110 (2019).
- Tiwary, P., Limongelli, V., Salvalaglio, M. & Parrinello, M. Kinetics of protein–ligand unbinding: Predicting pathways, rates, and rate-limiting steps. *Proc. Natl. Acad. Sci. USA* **112**, E386–E391 (2015).
- Bryant, D. & Moulton, V. Neighbor-net: an agglomerative method for the construction of phylogenetic networks. *Mol. Biol. Evol.* **21**, 255–265 (2004).
- Mullen, R. G., Shea, J.-E. & Peters, B. Transmission Coefficients, Committers, and Solvent Coordinates in Ion-Pair Dissociation. *J. Chem. Theory Comput.* **10**, 659–667 (2014).
- Sørensen, M. R. & Voter, A. F. Temperature-accelerated dynamics for simulation of infrequent events. *J. Chem. Phys.* **112**, 9599–9606 (2000).
- Guillain, F. & Thusius, D. Use of proflavine as an indicator in temperature-jump studies of the binding of a competitive inhibitor to trypsin. *J. Am. Chem. Soc.* **92**, 5534–5536 (1970).
- Amaral, M. *et al.* Protein conformational flexibility modulates kinetics and thermodynamics of drug binding. *Nat. Commun.* **8**, 2276 (2017).
- Hughes, I. & Hase, T. *Measurements and Their Uncertainties. A Practical Guide to Modern Error Analysis* (Oxford University Press, 2010).
- Geissler, P. L., Dellago, C. & Chandler, D. Kinetic Pathways of Ion Pair Dissociation in Water. *J. Phys. Chem. B* **103**, 3706–3710 (1999).
- Daldrop, J. O., Kowalik, B. G. & Netz, R. R. External potential modifies friction of molecular solutes in water. *Phys. Rev. X* **7**, 041065 (2017).

- <sup>40</sup>Hegger, R. & Stock, G. Multidimensional Langevin modeling of biomolecular dynamics. *J. Chem. Phys.* **130**, 034106 (2009).
- <sup>41</sup>Schaudinnus, N., Lickert, B., Biswas, M. & Stock, G. Global Langevin model of multidimensional biomolecular dynamics. *J. Chem. Phys.* **145**, 184114 (2016).
- <sup>42</sup>Marquart, M., Walter, J., Deisenhofer, J., Bode, W. & Huber, R. The geometry of the reactive site and of the peptide groups in trypsin, trypsinogen and its complexes with inhibitors. *Acta Crystallogr. B* **39**, 480–490 (1983).
- <sup>43</sup>Schiebel, J. *et al.* Intriguing role of water in protein-ligand binding studied by neutron crystallography on trypsin complexes. *Nat. Commun.* **9**, 166 (2018).
- <sup>44</sup>Buch, I., Giorgino, T. & De Fabritiis, G. Complete reconstruction of an enzyme-inhibitor binding process by molecular dynamics simulations. *Proc. Natl. Acad. Sci. USA* **108**, 10184–10189 (2011).
- <sup>45</sup>Plattner, N. & Noé, F. Protein conformational plasticity and complex ligand-binding kinetics explored by atomistic simulations and Markov models. *Nat. Commun.* **6**, 7653 (2015).
- <sup>46</sup>Votapka, L. W., Jagger, B. R., Heyneman, A. & Amaro, R. E. SEEKR: simulation enabled estimation of kinetic rates, a computational tool to estimate molecular kinetics and its application to trypsin–benzamidine binding. *J. Phys. Chem. B* **121**, 3597–3606 (2017).
- <sup>47</sup>Betz, R. M. & Dror, R. O. How Effectively Can Adaptive Sampling Methods Capture Spontaneous Ligand Binding? *J. Chem. Theory Comput.* **15**, 2053–2063 (2019).
- <sup>48</sup>Efron, B. & Stein, C. The Jackknife Estimate of Variance. *Ann. Stat.* **9**, 586–596 (1981).
- <sup>49</sup>Wolf, S. *et al.* Estimation of Protein-Ligand Unbinding Kinetics Using Non-Equilibrium Targeted Molecular Dynamics Simulations. *J. Chem. Inf. Model.* **59**, 5135–5147 (2019).
- <sup>50</sup>Kokh, D. B. *et al.* Estimation of Drug-Target Residence Times by  $\tau$ -Random Acceleration Molecular Dynamics Simulations. *J. Chem. Theory Comput.* **14**, 3859–3869 (2018).
- <sup>51</sup>Schuetz, D. A. *et al.* Predicting Residence Time and Drug Unbinding Pathway through Scaled Molecular Dynamics. *J. Chem. Inf. Model.* **59**, 535–549 (2019).
- <sup>52</sup>Capelli, R. *et al.* On the accuracy of molecular simulation-based predictions of koff values: a Metadynamics study. *bioRxiv* 2020.03.30.015396 (2020).
- <sup>53</sup>Nunes-Alves, A., Kokh, D. B. & Wade, R. C. Recent progress in molecular simulation methods for drug binding kinetics. *arXiv* 2002.08983 (2020). 2002.08983.
- <sup>54</sup>Casasnovas, R., Limongelli, V., Tiwary, P., Carloni, P. & Parrinello, M. Unbinding Kinetics of a p38 MAP Kinase Type II Inhibitor from Metadynamics Simulations. *J. Am. Chem. Soc.* **139**, 4780–4788 (2017).
- <sup>55</sup>Abraham, M. J. *et al.* Gromacs: High performance molecular simulations through multi-level parallelism from laptops to supercomputers. *SoftwareX* **1**, 19 – 25 (2015).
- <sup>56</sup>Hornak, V. *et al.* Comparison of multiple Amber force fields and development of improved protein backbone parameters. *Proteins* **65**, 712–725 (2006).
- <sup>57</sup>Best, R. B. & Hummer, G. Optimized molecular dynamics force fields applied to the helix-coil transition of polypeptides. *J. Phys. Chem. B* **113**, 9004–9015 (2009).
- <sup>58</sup>Jorgensen, W. L., Chandrasekhar, J., Madura, J. D., Impey, R. W. & Klein, M. Comparison of simple potential functions for simulating liquid water. *J. Chem. Phys.* **79**, 926 (1983).
- <sup>59</sup>Bussi, G. & Parrinello, M. Accurate sampling using Langevin dynamics. *Phys. Rev. E* **75**, 2289–7 (2007).

## Acknowledgements

We thank Peter Hamm and Matthias Post for numerous instructive and helpful discussions. The authors acknowledge support by the Deutsche Forschungsgemeinschaft (Sto 247/11), by the bwUniCluster computing

initiative, the High Performance and Cloud Computing Group at the Zentrum für Datenverarbeitung of the University of Tübingen, the state of Baden-Württemberg through bwHPC and the Deutsche Forschungsgemeinschaft through grant No. INST 37/935-1 FUGG.

## Author contributions

S.W. and G.S. designed and supervised research. S.W. performed TMD and Langevin simulations and nonequilibrium path separation of Trypsin trajectories. B.L. performed dLE analysis and implemented Langevin simulations. S.B. performed the nonequilibrium path separation of Hsp90 trajectories. All authors wrote the manuscript.

**Correspondence and requests for materials** should be addressed to S.W. and G.S.

## SUPPLEMENTARY INFORMATION

### SUPPLEMENTARY METHODS

#### MD simulation details.

Protein and ion interactions were described by the Amber99SB\* force field<sup>1,2</sup>, water molecules with the TIP3P model<sup>3</sup>. Simulations were carried out using Gromacs v2018 (Ref. 4) in a CPU/GPU hybrid implementation. Protein protonation states were evaluated with propka<sup>5</sup>. Van der Waals interactions were calculated with a cut-off of 1 nm, electrostatic interactions using the particle mesh Ewald method<sup>6</sup> with a minimal real-space cut-off of 1 nm. All covalent bonds with hydrogen atoms were constrained using LINCS<sup>7</sup>. After an initial steepest descent minimisation with positional restraints on protein and ligand heavy atoms, an initial 0.1 ns equilibration MD simulation in the NPT ensemble was performed with a 1 fs time step and positional restraints of protein and ligand heavy atoms. A temperature of 290.15 K was kept constant using the Bussi (v-rescale) thermostat<sup>8</sup> (coupling time constant of 0.2 ps), the pressure was kept constant at 1 bar using the Berendsen barostat<sup>9</sup> (coupling time constant of 0.5 ps), followed by a second steepest descent minimisation without restraints and a short 0.1 ns equilibration MD simulation in the NPT ensemble.

dcTMD calculations<sup>10</sup> were carried out using the PULL code implemented in Gromacs using the "constraint" option employing a SHAKE implementation<sup>11</sup>. 200–400 statistically independent start points of simulations were obtained by generating different atomic velocity distributions after the 10 ns unbiased simulations, all corresponding to a temperature of 290.15 K. After a 0.1 ns preequilibration using parameters as described above with positional restraints on protein and ligand heavy atoms and a constant distance constraint of all simulation systems, constant velocity calculations were carried out with  $v_c = 1$  m/s covering a distance of 2 nm, switching the barostat to the Parrinello-Rahman barostat<sup>12</sup>. The constraint pseudo-force  $f_c$  was written out each time step.

**NaCl.** Free energy  $\Delta G(x)$  and friction profiles  $\Gamma(x)$  were obtained from 1000 trajectories of previous dcTMD calculations<sup>10</sup> at pulling velocity  $v_c = 1$  m/s. For a better sampling, we continued the unbiased fully atomistic simulations described in Ref. 10 and extended them to a full microsecond of simulated time. As these simulations used a cubic simulation box, binding and unbinding waiting times cannot directly be compared to the results of our Langevin simulation with "reflective" borders (see below), which represent radial dynamics. To obtain data sets that allow such a comparison, we removed all time steps with  $x < 0.265$  nm and  $x > 1.265$  nm from MD trajectories, and calculated mean waiting times for the resulting cut  $x(t)$  trajectories.

**Trypsin-benzamidine.** Benzamidine parameters were obtained using Antechamber<sup>13</sup> and Acypype<sup>14</sup> with atomic parameters derived from GAFF parameters<sup>15</sup>. Atomic charges were obtained as RESP charges<sup>16</sup> based on QM calculations at the HF/6-31G\* level using Orca<sup>17</sup> and Multiwfn<sup>18</sup>. Trypsin (PDB ID 3PTB)<sup>19</sup> was placed into a dodecahedral box with dimensions of 7.5 x 7.5 x 5.3 nm<sup>3</sup> side length and solvated with 8971 water molecules. 16 sodium and 25 chloride ions were added to yield a charge neutral box with a salt concentration of 0.1 M<sup>20</sup>. After the initial equilibration, we added an additional 10 ns unbiased MD simulation to yield a converged protein structure. As pulling coordinates, we used the distance between the center of mass of all benzamidine heavy atoms and the one of the C $_{\alpha}$  atoms of the central  $\beta$ -sheet of trypsin.

**Hsp90-inhibitor.** Parameters of the resorcinol inhibitor were taken from Ref. 21: here, inhibitor parameters were generated using Antechamber<sup>13</sup> and Acypype<sup>14</sup> with atomic parameters derived from GAFF parameters<sup>15</sup> and AM1-BCC atomic charges<sup>22,23</sup>. Solvated simulation boxes of the Hsp90-inhibitor complex were taken from Ref. 21 (compound **1j**), which in turn are based on the 2.5 Å X-ray crystal structure with PDB ID 6FCJ<sup>24</sup>. As in the case of trypsin, the distance between the center of mass of all ligand heavy atoms and the one of the C $_{\alpha}$  atoms of the central

$\beta$ -sheet of Hsp90 served as as pulling coordinate as used in Ref. 21.

**Data evaluation.** Minimal distance evaluation for contact determination was performed using the MDAnalysis Python library<sup>25</sup>, nonequilibrium principal component analysis was carried out using the fastpca program<sup>26</sup>. Data evaluation was carried out using a Jupyter notebook<sup>27</sup> employing the numpy<sup>28</sup>, scipy<sup>29</sup> and astropy<sup>30</sup> Python libraries. Graphs were plotted using the matplotlib<sup>31</sup> Python library, molecular structures were displayed via PyMOL<sup>32</sup>.

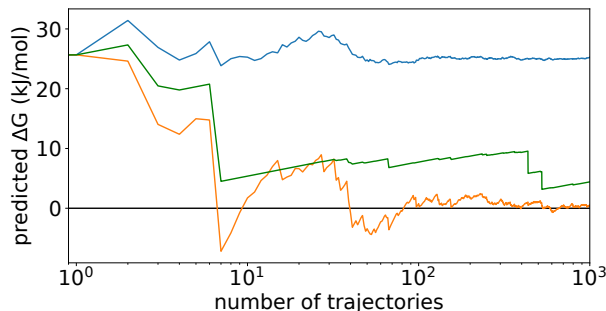


FIG. S5. **Convergence of dcTMD free energy estimate**, illustrated for a Gaussian work distribution. Compared are  $\langle W \rangle$  in blue,  $\Delta G$  estimate by Jarzynski's identity in green, cumulant expansion estimate in orange.

### Statistical convergence of dcTMD free energy and friction estimates

To illustrate the statistical convergence of various quantities (such as mean work and free energy) calculated via the second-order cumulant expansion of Jarzynski's identity, we have performed a detailed study for a large range of ensemble sizes and pulling velocities in the case of NaCl (see the Supplementary Information of Ref. 10). Using a simple model problem, here we restrict us to demonstrate the clear improvement of the convergence behavior when the second-order cumulant expansion instead of the direct evaluation of Jarzynski's identity is used. To this end, we generated test data in form of draws from a normal distribution with mean  $\langle W \rangle$  and variance  $\langle \delta W^2 \rangle$  chosen such that  $\Delta G = \langle W \rangle - \frac{1}{2k_B T} \langle \delta W^2 \rangle = 0$ . As Supplementary Fig. S5 shows, the estimator from Jarzynski's identity exhibits a slow, erratic convergence behavior. On the other hand, the cumulant expansion-based estimator gives the dissipated work in terms of the variance of the nonequilibrium work, which is much easier to compute and converges to a fluctuation around  $1k_B T \approx 2.5$  kJ/mol after  $\sim 100$  draws.

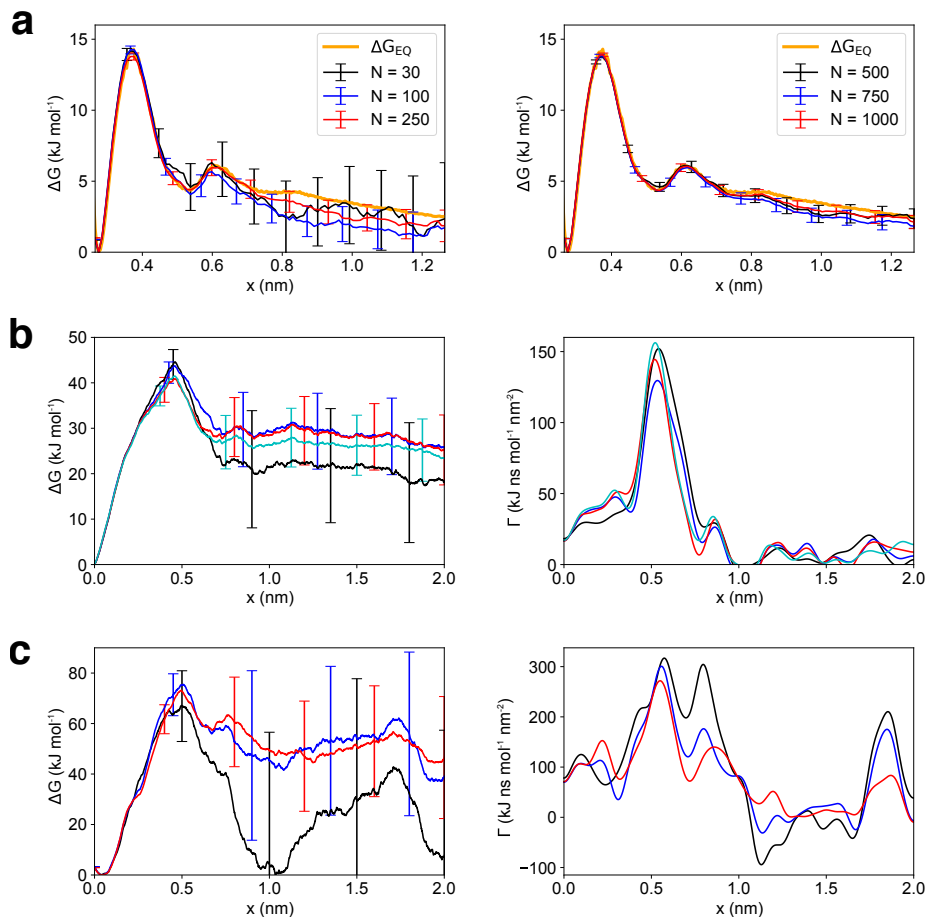


FIG. S6. Jackknife analysis of free energy profiles and Gauss-smoothed friction ( $\sigma = 40$  ps), as obtained for **a** NaCl-water, **b** trypsin-benzamidine, and **c** Hsp90-inhibitor complex. Error bars denote the Jackknife standard error obtained for various numbers of TMD trajectories ("samples"). Color code in **b**: 52 samples in black, 84 in blue, 117 in red, 148 in cyan. Color code in **c**: 30 in black, 50 in blue, 93 in red.

In a similar vein, we analyzed the convergence of free energies and friction profiles in our three molecular simulation systems. To estimate an error of the free energy profiles, we resort to a Jackknife ("leave-one-out") analysis<sup>33</sup>, which represents a superior method if we do not know the distribution that the free energy estimate follows. Because the estimate of the free energy depends on the estimate of both mean and variance of the nonequilibrium work (see the Theory section in the main text), the error of the free energy will decrease with the error of the 2<sup>nd</sup> moment of the nonequilibrium work, which is known to converge slowly<sup>34</sup>. Consequentially, while we expect the estimate of the mean free energy to converge comparatively fast, the error will converge slower.

Figure S6 displays the convergence of free energies and friction profiles of NaCl-water and the two investigated protein-ligand systems. In the case of the NaCl system, the free energy is within  $1 k_B T$  of the free energy from unbiased simulations directly for  $N=30$  simulations, while the error decreases to below  $1 k_B T$  within  $N=100$  simulations. Please see the Supplementary Information of Ref. 10 for the convergence of NaCl-water friction factors. For the trypsin-benzamidine system, free energies appear to converge with  $\sim 100$  trajectories, despite an error of  $\sim 4 k_B T$ . In a similar vein, the free energy estimates for the Hsp90-inhibitor complex change for  $\sim 2 k_B T$  after  $\sim 100$  trajectories. A similar convergence appears to apply to friction fields. We therefore expect about 100 trajectories per path to be sufficient to obtain a sufficiently converged free energy surface and friction profile for rate prediction.

Furthermore, the binding free energies of  $\sim 27$  kJ/mol (Trypsin) and  $\sim 45$  kJ/mol (Hsp90), calculated as the

difference between  $\Delta G$  at  $x = 0$  nm and  $x = 2$  nm, compare well to the standard free energies of binding  $\Delta G^0 = 28.0$  kJ/mol (Ref. 20) and  $40.7 \pm 0.2$  kJ/mol (Ref. 35), respectively, based on the experimentally measured  $K_D = C_0 \exp(-\Delta G^0/k_B T)$  with the standard reference concentration  $C_0 = 1$  mol/l. We are aware that a distance-based free energy difference as used here and a standard free energy of binding can differ by several  $k_B T$  (see Ref. 36). We therefore base the goodness of our predictions in the main text on protein-ligand complex rates and the resulting  $K_D$ , respectively.

Lastly, we note that the convergence is best and errors are smallest directly around the main barrier. Therefore, predictions of unbinding rates will be more accurate than predictions of binding rates, despite being the slower and thus actually harder rate to predict.

### Pathway separation

In the case of trypsin-benzamidine, pathway separation was performed by employing nonequilibrium principal component analysis<sup>37</sup> (PCA) using a covariance matrix based on protein-ligand contact distances<sup>38</sup>. To this end, the PCA included all minimal amino acid-ligand distances that are found below a cut-off distance of 4.5 Å in any snapshot of all pulling trajectories. Trajectories were projected onto the first two principal components and sorted according to pathways by visual inspection as displayed in Supplementary Fig. S7. dcTMD calculations of free energy and friction were then carried out separately for such bundles of trajectories. Performing 200 pulling simulations of trypsin-benzamidine, we found 84 trajectories to constitute the major unbinding pathway ("middle" pathway in Fig. S7), for which free energy and friction profiles were converged, and whose free energy difference between bound and unbound state qualitatively agree with the standard free energy of binding known from experiment (see Supplementary Fig. S6).

For the Hsp90-inhibitor complex, we employed a path separation based on geometric distances between individual trajectories<sup>39</sup>. After aligning trajectories with the protein's  $C_\alpha$  atoms as fit reference, we calculated the matrix of means over time of the root mean square distance of ligand heavy atoms between individual trajectories. We then applied the NeighborNet algorithm<sup>40</sup> to the matrix to cluster trajectories according to distances. From the considered 400 trajectories, the cluster that gave a free energy difference between  $x = 0$  nm and  $x = 2$  nm that was closest to the experimental  $\Delta G^0$  calculated from the respective  $K_D$ <sup>35</sup> was taken by 93 single trajectories.

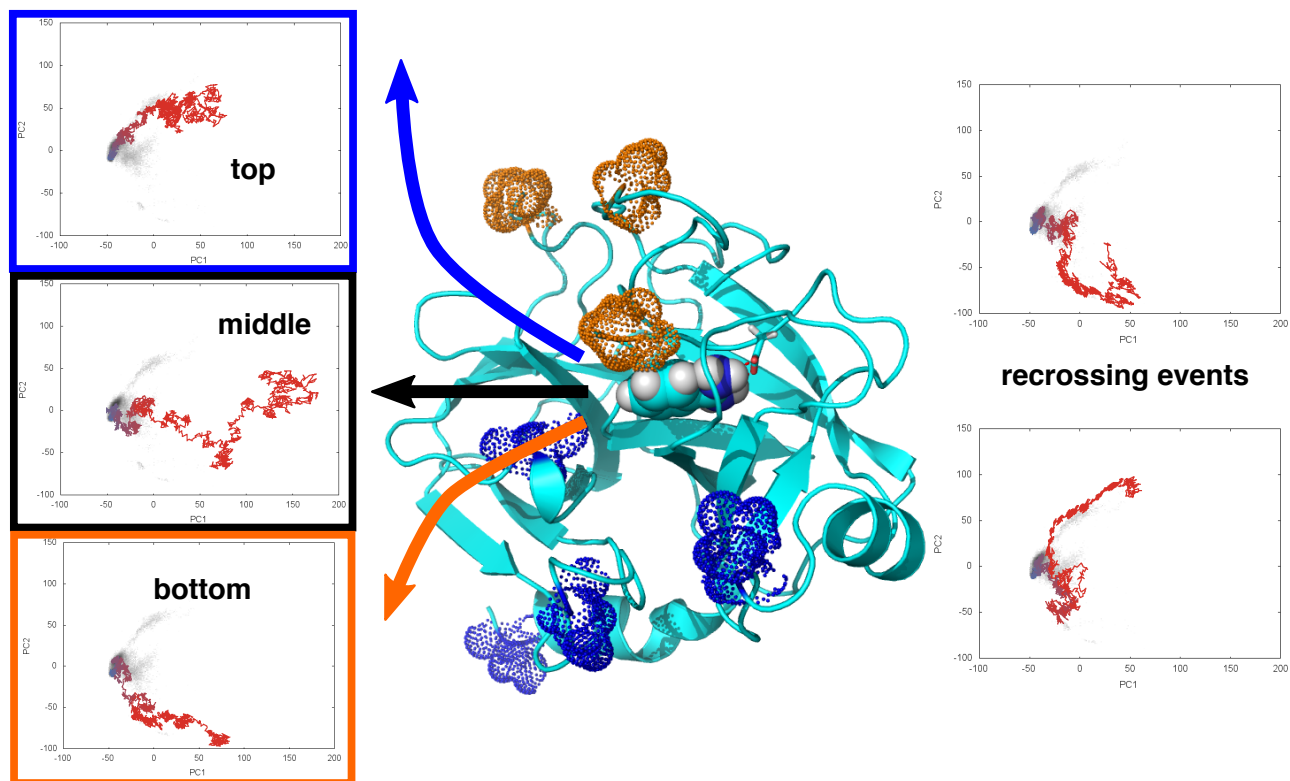


FIG. S7. Pathways predicted by dcTMD for the unbinding of trypsin-benzamidine, using a pulling velocity of  $v_c = 1$  m/s. (Middle) Structure of trypsin (PDB ID 3PTB)<sup>19</sup> as cartoon, benzamidine as van der Waals spheres, Asp189 in sticks, residues characterizing PC2 as blue and orange dots, respectively. Arrows indicate the direction of pathways. (Left) Nonequilibrium PCA results display minima in nonequilibrium energies as grey shades, corresponding to temporary binding sites during unbinding. Projected single representative trajectories as lines are colored from blue to red according to time evolution. All trajectories start from a central minimum at  $(-50,0)$ . Three main pathways (top, middle, bottom) can be observed: the "top" pathway passes through the elongated minimum at  $(0,50)$ , the "middle" pathway through the central minimum around  $(-25,0)$ , and the "bottom" pathway through a shallow minimum at ca.  $(-10,-70)$ . The "middle" pathway is majorly populated. (Right) Additionally, trajectories can "re-cross" between the pathways: in the presented examples, trajectories first follow the "middle" pathway before crossing over to the "bottom" pathway at  $PC1 \approx -20$  nm (top) or jump between all three pathways at once (bottom).

### Optimal pulling velocities

While the results presented above display the evaluation of single pathways after a successful pathway separation, being able to do so depends on finding a suitable pulling velocity  $v_c$  that allows to distinguish pathways. To obtain a nonequilibrium work profile that contains the least dissipative work and at the same time uses the most likely pathway between states, it intuitively appears to be the best choice to pull as slowly as possible. Supplementary Figure S8 displays nonequilibrium energy landscapes<sup>37</sup> obtained from dcTMD simulations of the trypsin-benzamidine complex, using 100 trajectories at  $v_c = 0.1, 1$  and  $10$  m/s. We recognise a tradeoff between the pulling velocity and the structural resolution of the associated energy landscape. For  $10$  m/s, we hardly observe any structure in the first two PCs. Though this velocity is suited for a scoring of ligands according to unbinding kinetics<sup>21</sup>, obviously a pathway separation cannot be performed. For  $1$  m/s, we observe several intermediate states in the nonequilibrium energy profile along the first two PCs. While the structure in the first two PCs becomes better resolved in simulations with  $0.1$  m/s pulling velocity, sorting trajectories into unique pathways becomes unfeasible due the dominance of recrossing events between the pathways (Supplementary Fig. S7). This finding can be explained by assuming that

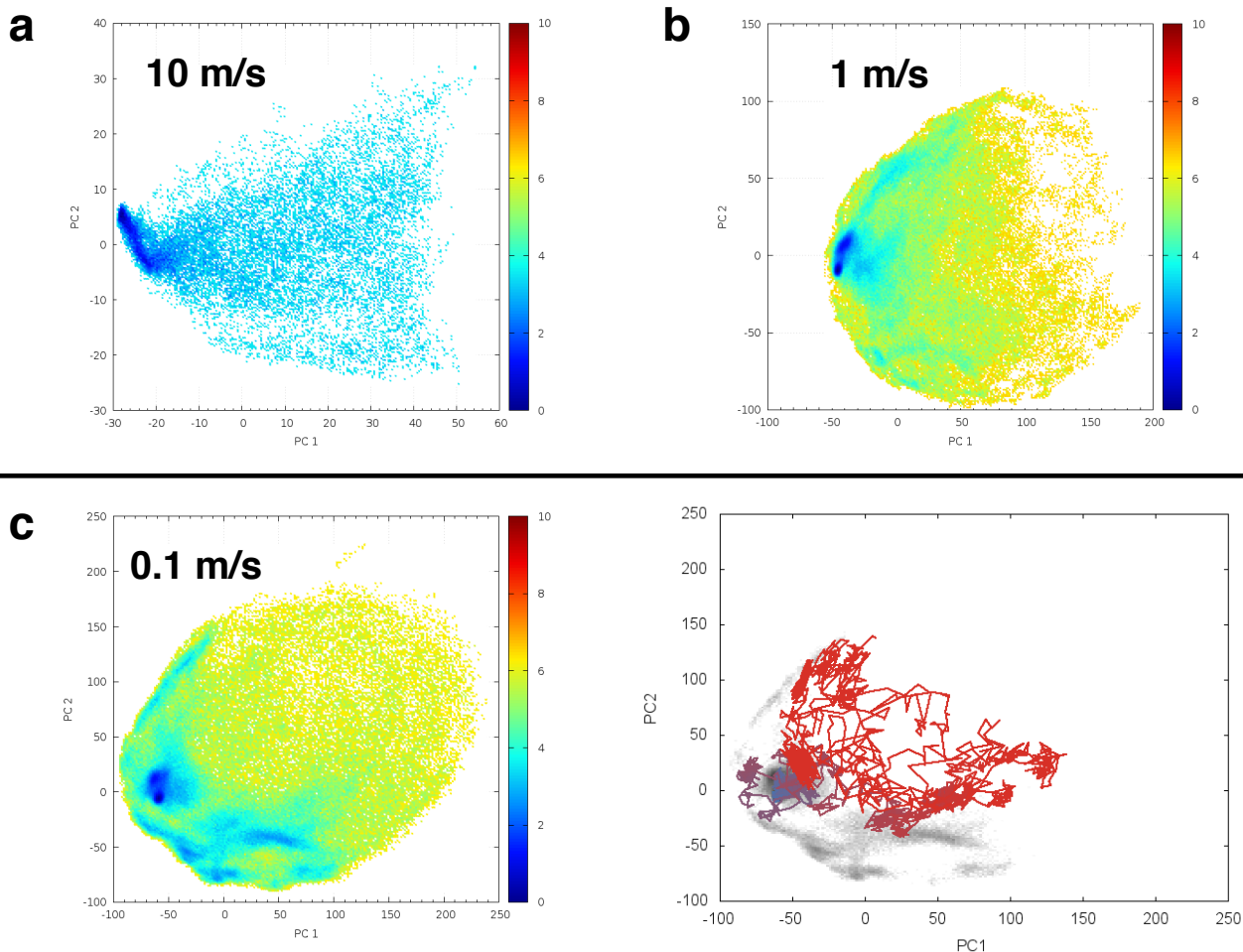


FIG. S8. **Velocity dependence of pathways in dcTMD simulations** Nonequilibrium energy landscapes  $\Delta\mathcal{G}(PC1, PC2) = -k_B T P(PC1, PC2)$  obtained from dcTMD simulations of the trypsin-benzamidine complex, where  $P(PC1, PC2)$  is the probability distribution of all dcTMD simulations projected on the first two principal components of a contact distance PCA<sup>37</sup>. For  $v_c = 10$  m/s (a), no pathways are present, while for 1 m/s (b) structures corresponding to pathways appear. At 0.1 m/s (c), a number of local energy minima appear, that reflect a multitude of pathways present. A pathway separation becomes impossible, as recrossing events dominate (see Supplementary Fig. S7).

single transitions over barriers, as we try to enforce by applying constraints, take place on a natural timescale between pico- and nanoseconds<sup>41</sup>. Forcing the system over such barriers on a time scale that is too long, i.e., with a too slow velocity, causes an artificial stationarity, resulting in the ligand accessing side states on top of or close to the barrier, which in equilibrium would not be accessed, and influence from protein conformational fluctuations. As a consequence, application of dcTMD to "real world" systems comes at the price of needing to identify such "goldilocks" velocities, with 1 m/s being a good rule of thumb velocity.

## Langevin simulations

Langevin simulations used the integration scheme by Bussi and Parrinello<sup>8</sup>. Simulations were run for 1  $\mu$ s of simulation time for NaCl at temperatures between 293 to 420 K, and 10 ms for the two protein-ligand systems, using temperatures 380 to 900 K for trypsin-benzamidine and 700 to 1350 K for the Hsp90-inhibitor complex. As system mass  $m$ , the reduced mass of the NaCl dimer (13.88 g/mol), the trypsin-benzamidin (120.15 g/mol) and Hsp90-inhibitor (288.73 g/mol) complexes were used. System coordinates were written out each 1 ps for NaCl and each 1 ns for the protein-ligand systems.

TABLE S1. Convergence of the Bussi-Parrinello integration scheme<sup>8</sup> of the Langevin equation with respect to the integration time step  $\Delta t$  and the mass  $m$  used in the Langevin equation. The first table shows dissociation and association times obtained from 10 simulations of NaCl at  $T = 293$  K over 1  $\mu$ s simulated time, as well as results from a 1  $\mu$ s long MD simulation. The other two tables show results obtained for 5 simulations of trypsin-benzamidine at  $T = 800$  K over 0.2 ms simulated time, and 5 simulations of Hsp90-inhibitor complex at  $T = 1200$  K over 0.2 ms simulated time, respectively. Errors denote the standard error of the mean.

<b>NaCl</b>		normal mass		mass $\times 10$	
$\Delta t$ (fs)	$\tau_{\text{diss}}$ (ps)	$\tau_{\text{assoc}}$ (ps)	$\tau_{\text{diss}}$ (ps)	$\tau_{\text{assoc}}$ (ps)	
0.1	406 $\pm$ 8	3,248 $\pm$ 66	464 $\pm$ 7	3,580 $\pm$ 50	
0.2	404 $\pm$ 8	3,174 $\pm$ 63	467 $\pm$ 12	3,528 $\pm$ 80	
0.5	411 $\pm$ 8	3,166 $\pm$ 65	457 $\pm$ 9	3,392 $\pm$ 48	
1.0	428 $\pm$ 9	3,157 $\pm$ 65	448 $\pm$ 8	3,266 $\pm$ 78	
2.0	403 $\pm$ 8	3,162 $\pm$ 63	449 $\pm$ 8	3,353 $\pm$ 39	
5.0	420 $\pm$ 9	3,035 $\pm$ 61	468 $\pm$ 13	3,454 $\pm$ 53	
10.0	345 $\pm$ 6	2,631 $\pm$ 47	452 $\pm$ 10	3,512 $\pm$ 71	
20.0	249 $\pm$ 5	1,907 $\pm$ 25	468 $\pm$ 10	3,475 $\pm$ 67	
MD	124 $\pm$ 6	848 $\pm$ 47	124 $\pm$ 6	848 $\pm$ 47	
<b>Trypsin</b>		normal mass		mass $\times 10$	
$\Delta t$ (fs)	$\tau_{\text{diss}}$ (ns)	$\tau_{\text{assoc}}$ (ns)	$\tau_{\text{diss}}$ (ns)	$\tau_{\text{assoc}}$ (ns)	
0.5	111 $\pm$ 2	32 $\pm$ 1	112 $\pm$ 3	33 $\pm$ 1	
1.0	106 $\pm$ 2	32 $\pm$ 1	111 $\pm$ 1	34 $\pm$ 1	
2.0	96 $\pm$ 3	28 $\pm$ 1	111 $\pm$ 3	33 $\pm$ 1	
5.0	61 $\pm$ 2	18 $\pm$ 1	112 $\pm$ 5	33 $\pm$ 1	
10.0	37 $\pm$ 1	10 $\pm$ 1	105 $\pm$ 5	32 $\pm$ 1	
20.0	–	–	95 $\pm$ 4	28 $\pm$ 1	
<b>Hsp90</b>		normal mass		mass $\times 10$	
$\Delta t$ (fs)	$\tau_{\text{diss}}$ (ns)	$\tau_{\text{assoc}}$ (ns)	$\tau_{\text{diss}}$ (ns)	$\tau_{\text{assoc}}$ (ns)	
0.5	628 $\pm$ 25	60 $\pm$ 6	641 $\pm$ 36	61 $\pm$ 5	
1.0	635 $\pm$ 50	60 $\pm$ 4	638 $\pm$ 38	63 $\pm$ 6	
2.0	567 $\pm$ 18	56 $\pm$ 3	636 $\pm$ 35	63 $\pm$ 4	
5.0	356 $\pm$ 12	36 $\pm$ 2	621 $\pm$ 34	63 $\pm$ 6	
10.0	212 $\pm$ 8	20 $\pm$ 1	608 $\pm$ 21	60 $\pm$ 5	
20.0	–	–	545 $\pm$ 41	55 $\pm$ 4	

For each system, we studied the convergence of the Bussi-Parrinello integrator with respect to the time step  $\Delta t$ , see Table S1. We find that NaCl requires an integration time step of  $\Delta t \lesssim 5$  fs, while the protein-ligand systems require a significantly shorter time step of  $\Delta t \lesssim 1$  fs. Owing to the Fourier relation  $\Delta E \Delta t \sim \hbar$ , this finding is a consequence of the larger barrier height  $\Delta E$  of the free energy landscape of the protein-ligand systems.

To test if the dynamics is overdamped, Langevin simulations were repeated using a mass that is ten times larger than the normal reduced mass. (Overdamped dynamics neglects the inertia term and therefore does not depend on the mass<sup>42</sup>.) Since the resulting (un)binding times do not change for the protein-ligand systems, these systems are clearly overdamped. By using the enhanced mass, the protein-ligand systems can therefore be integrated by using a time step of  $\Delta t \lesssim 10$  fs, and therefore require an order of magnitude less simulation time. Moreover, the overdamped limit allows us to circumvent the definition of the effective mass associated with a given pulling coordinate, which depends on various technical issues such as the definition of the pulling centers. On the other hand, NaCl shows a 15 % increase of the dissociation and association times, and may be therefore classified as almost overdamped.

The gradient of the potential of mean force was approximated as

$$\frac{dG(x)}{dx} \approx \frac{[\Delta G(x + \Delta x) - \Delta G(x)] + [\Delta G(x) - \Delta G(x - \Delta x)]}{2\Delta x} \quad (\text{S05})$$

Input free energy and friction fields obtained from dcTMD were smoothed with a Gauss filter ( $\sigma = 10$  for NaCl and 40 ps for protein-ligand systems, respectively). In some cases, though, friction fields still exhibited negative values after smoothing, which we found to be a consequence of not completely converged friction profiles. The problem can be circumvented by improved sampling or an increased  $\sigma = 100$  ps, which we used in the preparation of Figures 3 and 4 in the main text. As workaround, we found that using the absolute values  $|\Gamma(x)|$  after smoothing with  $\sigma = 40$  ps as input for simulations is sufficient as well, provided that we have at least 80–100 trajectories available for a pathway of interest. This workaround was used to prepare fields for protein-ligand Langevin simulations. For  $x$ , we used a resolution of 1 pm. For compensation of data borders, we employed "fully reflective" boundary conditions: If the system jumped over a boundary  $x_{\max}$  at any time step by a distance  $a$ , it was put back to  $x = x_{\max} - a$ , and its velocity sign reversed.

Mean waiting times  $\tau$  were calculated by defining geometric cores<sup>43</sup>: For NaCl, the free energy surface was separated into the bound state  $x < 0.31$  nm and unbound state  $x > 0.43$ . For trypsin-benzamidine, we used a bound state  $x < 0.3$  nm and unbound state  $x > 0.6$  nm, while for the Hsp90-inhibitor complex, we applied cores of  $x < 0.3$  nm and  $x > 0.9$  nm. As the native units of  $k_{\text{on}}$  are  $\text{s}^{-1} \text{M}^{-1}$ , all according binding rates were scaled by a pulling coordinate-dependent reference concentration  $C = 1 / (\frac{4}{3}\pi x_{\text{ref}}^3)$  for one ion or protein-ligand pair with  $x_{\text{ref}} = x_{\text{end}} - x_0$ , amounting to a molarity of 0.2 M for NaCl Langevin simulations and 50 mM for protein-ligand Langevin simulations.

To demonstrate the effect of constraints used in dcTMD, Supplementary Figure S9 displays a comparison of friction fields of the NaCl-water system obtained from dcTMD and a data-driven Langevin equation (dLE)<sup>44</sup>. The latter uses no constraints, but calculates the friction via a local average<sup>44</sup>. The dLE was applied to 200 ns unbiased equilibrium MD data and the consistency of the  $\Gamma$  estimate was verified by comparing MD and dLE dynamics. While both fields differ in the details of shape, the dLE field reaches approximately the final friction value from dcTMD in the unbound state at maximal  $x$ . On average, we find that dcTMD clearly overestimates the friction, which presumably is caused by the moving position constraints<sup>45</sup>.

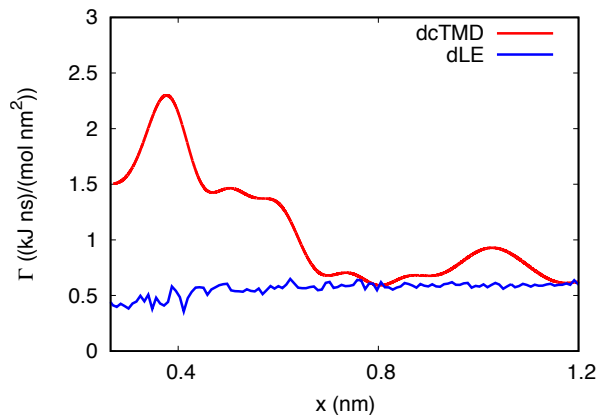


FIG. S9. **Comparison of friction estimates.** Friction calculated from a data-driven Langevin equation<sup>44</sup> in comparison to results from dcTMD, obtained for the example of NaCl in water.

### Uncertainty for prediction of rates with temperature boosting

To estimate the extrapolation error of  $T$ -boosting, we assume that the waiting time  $\tau$  of an unbinding or binding process is exponentially distributed,

$$P(\tau) = \frac{1}{\langle\tau\rangle} e^{-\frac{\tau}{\langle\tau\rangle}}, \quad (\text{S06})$$

where  $\langle\tau\rangle$  is a function of the temperature  $T$ . Hence the expectation  $\bar{\tau}$  is given by its mean  $\langle\tau\rangle$  plus/minus the error of the mean

$$\bar{\tau}(T) = \langle\tau(T)\rangle \pm \frac{\langle\tau(T)\rangle}{\sqrt{N(T)}}, \quad (\text{S07})$$

where  $N(T)$  denotes the number of simulated transitions. By changing to the dimensionless rate  $k = t_0/\langle\tau\rangle$  (with  $t_0$  being some timescale, e.g., ns) and employing Gaussian error propagation to lowest order<sup>46</sup>, we obtain accordingly

$$\ln(\bar{k}(T)) = \ln(k(T)) \pm \frac{1}{\sqrt{N(T)}}. \quad (\text{S08})$$

Due to the rate expression  $k \propto e^{-\Delta G/k_B T}$  with transition state energy  $\Delta G$ ,  $\ln(k)$  depends linearly on  $1/T$ , i.e.,

$$\ln(k(T)) = \frac{a}{T} + b. \quad (\text{S09})$$

Linear regression theory<sup>46</sup> yields estimates for  $a$  and  $b$  as well as uncertainties

$$\sigma_b = \sqrt{\frac{\sum_i \frac{N(T_i)}{T_i^2}}{\Delta}} \quad (\text{S010})$$

and

$$\sigma_a = \sqrt{\frac{\sum_i N(T_i)}{\Delta}} \quad (\text{S011})$$

with

$$\Delta = \sum_i N(T_i) \sum_i \frac{N(T_i)}{T_i^2} - \left( \sum_i \frac{N(T_i)}{T_i} \right)^2, \quad (\text{S012})$$

where  $T_i$  denotes a discrete set of temperatures at which simulations are performed. Employing error propagation, we estimate the uncertainty of  $\ln(k)$  at  $T_{\text{ref}} = 300$  K as

$$\sigma_{\ln(k(T_{\text{ref}}))} = \sqrt{\left(\frac{\sigma_a}{T_{\text{ref}}}\right)^2 + \sigma_b^2}. \quad (\text{S013})$$

This yields for the desired relative uncertainty of the average waiting time

$$\bar{\tau}(T_{\text{ref}}) = \langle \tau(T_{\text{ref}}) \rangle \pm \langle \tau(T_{\text{ref}}) \rangle \cdot \sigma_{\ln(k(T_{\text{ref}}))}. \quad (\text{S014})$$

To illustrate the typical magnitude of this uncertainty, we assume that we perform 10 Langevin simulations of length  $t_{\text{LE}}$  at different temperatures  $T_i$  ( $i = 0, \dots, 9$ )

$$T_i = T_0 + i \left( 25 \frac{T_0}{T_{\text{ref}}} \right) \text{K}. \quad (\text{S015})$$

The first three temperatures ( $T_0$ ,  $T_1$  and  $T_2$ ) are chosen such that we observe  $\approx 10^2$  transitions during the simulation time  $t_{\text{LE}}$ . Similarly, we assume to observe  $10^3$  transitions at  $T_3$ ,  $T_4$  and  $T_5$ ,  $10^4$  transitions at  $T_6$ ,  $T_7$  and  $T_8$  and  $10^5$  transitions at  $T_9$ . Using the case of  $T_0 = T_{\text{ref}} = 300$  K, since we assumed  $10^2$  transitions at  $T_0 = T_{\text{ref}}$  during the Langevin simulation time  $t_{\text{LE}}$ , the observed rate at 300 K is  $k = 10^2/t_{\text{LE}}$ . Choosing  $t_{\text{LE}} = 5$  ms, the corresponding rate is  $k(300\text{K}) = 1/50\mu\text{s}$ , and we obtain for the error of the rate  $\sigma_{\ln(k(T_{\text{ref}}))} = 7.7\%$ . Alternatively, when we assume that we need to choose  $T_0 \approx 450$  K in order to achieve  $10^2$  transitions, employing the boosting relation (4) in the main text and  $t_{\text{LE}} = 5$  ms, the observed rate at 300 K is  $k(300\text{K}) = 0.063 \text{ ms}^{-1}$  with an error of 10.6%.

Considering our Langevin simulations of trypsin described in the main text, where we used  $T$ -boosting at 13 temperatures from 380–900 K, the error at 300 K is estimated to be  $\sigma_{\ln(k(T_{\text{ref}}))} = 3.3\%$ . For Hsp90, the system with the highest considered barrier, we obtain  $\sigma_{\ln(k(T_{\text{ref}}))} = 11.0\%$  at 300 K using Langevin simulations at 14 temperatures from 700–1350 K. As the overestimation of friction factors due to usage of constraints (see main text) results in an underestimation of rates by a factor of  $\sim 4$ , and as the error of free energy profiles enters Eq. [4] in the exponent, the extrapolation error due to  $T$ -boosting can easily be made negligible in all practical cases.

- <sup>1</sup>V. Hornak, R. Abel, A. Okur, B. Strockbine, A. Roitberg, and C. Simmerling, Comparison of multiple Amber force fields and development of improved protein backbone parameters, *Proteins* **65**, 712 (2006).
- <sup>2</sup>R. B. Best and G. Hummer, Optimized molecular dynamics force fields applied to the helix-coil transition of polypeptides, *J. Phys. Chem. B* **113**, 9004 (2009).
- <sup>3</sup>W. L. Jorgensen, J. Chandrasekhar, J. D. Madura, R. W. Impey, and M. Klein, Comparison of simple potential functions for simulating liquid water, *J. Chem. Phys.* **79**, 926 (1983).
- <sup>4</sup>M. J. Abraham, T. Murtola, R. Schulz, S. Pall, J. C. Smith, B. Hess, and E. Lindahl, Gromacs: High performance molecular simulations through multi-level parallelism from laptops to supercomputers, *SoftwareX* **1**, 19 (2015).
- <sup>5</sup>M. H. Olsson, C. R. S ndergaard, M. Rostkowski, and J. H. Jensen, PROPKA3: consistent treatment of internal and surface residues in empirical p K a predictions, *J. Chem. Theory Comput.* **7**, 525 (2011).
- <sup>6</sup>T. Darden, D. York, and L. Petersen, Particle mesh Ewald: An N log(N) method for Ewald sums in large systems, *J. Chem. Phys.* **98**, 10089 (1993).
- <sup>7</sup>B. Hess, H. Bekker, H. J. C. Berendsen, and J. G. E. M. Fraaije, LINCS: A linear constraint solver for molecular simulations, *J. Comp. Chem.* **18**, 1463 (1997).
- <sup>8</sup>G. Bussi, D. Donadio, and M. Parrinello, Canonical sampling through velocity rescaling, *J. Chem. Phys.* **126**, 014101 (2007).
- <sup>9</sup>H. J. C. Berendsen, J. P. M. Postma, W. F. van Gunsteren, A. Dinola, and J. R. Haak, Molecular dynamics with coupling to an external bath, *J. Chem. Phys.* **81**, 3684 (1984).
- <sup>10</sup>S. Wolf and G. Stock, Targeted molecular dynamics calculations of free energy profiles using a nonequilibrium friction correction, *J. Chem. Theory Comput.* **14**, 6175 (2018).
- <sup>11</sup>J. P. Ryckaert, G. Cicotti, and H. J. C. Berendsen, Numerical-integration of cartesian equations of motions of a system with constraints-molecular dynamics of n-alkanes, *J. Comput. Phys.* **23**, 327 (1977).
- <sup>12</sup>M. Parrinello and A. Rahman, Polymorphic transitions in single crystals: A new molecular dynamics method, *J. Appl. Phys.* **52**, 7182 (1981).
- <sup>13</sup>J. Wang and R. Br uschweiler, 2D entropy of discrete molecular ensembles, *J. Chem. Theory Comput.* **2**, 18 (2006).
- <sup>14</sup>A. W. Sousa da Silva and W. F. Vranken, ACPYPE - AnteChamber PYthon Parser interfacE, *BMC Res. Notes* **5**, 367 (2012).
- <sup>15</sup>J. M. Wang, R. M. Wolf, J. W. Caldwell, P. A. Kollman, and D. A. Case, Development and testing of a general amber force field, *J. Comput. Chem.* **25**, 1157 (2004).
- <sup>16</sup>C. I. Bayly, P. Cieplak, W. D. Cornell, and P. A. Kollman, A well-behaved electrostatic potential based method using charge restraints for deriving atomic charges: The resp model, *J. Phys. Chem.* **97**, 10269 (1993).
- <sup>17</sup>F. Neese, The ORCA program system, *WIREs Comput. Mol. Sci.* **2**, 73 (2012).
- <sup>18</sup>T. Lu and F. Chen, Multiwfn: A multifunctional wavefunction analyzer, *J. Comput. Chem.* **33**, 580 (2012).
- <sup>19</sup>M. Marquart, J. Walter, J. Deisenhofer, W. Bode, and R. Huber, The geometry of the reactive site and of the peptide groups in trypsin, trypsinogen and its complexes with inhibitors, *Acta Crystallogr. B* **39**, 480 (1983).
- <sup>20</sup>F. Guillain and D. Thusius, Use of proflavine as an indicator in temperature-jump studies of the binding of a competitive inhibitor to trypsin, *J. Am. Chem. Soc.* **92**, 5534 (1970).
- <sup>21</sup>S. Wolf et al., Estimation of Protein-Ligand Unbinding Kinetics Using Non-Equilibrium Targeted Molecular Dynamics Simulations., *J. Chem. Inf. Model.* **59**, 5135 (2019).
- <sup>22</sup>A. Jakalian, B. L. Bush, D. B. Jack, and C. I. Bayly, Fast, efficient generation of high-quality atomic Charges. AM1-BCC model: I. Method, *J. Comput. Chem.* **21**, 132 (2000).
- <sup>23</sup>A. Jakalian, D. B. Jack, and C. I. Bayly, Fast, efficient generation of high-quality atomic charges. AM1-BCC model - II. Parameterization and validation., *J. Comput. Chem.* **23**, 1623 (2002).
- <sup>24</sup>J. G ldenhaupt, M. Amaral, C. K tting, J. Schartner, D. Musil, M. Frech, and K. Gerwert, Ligand-Induced Conformational Changes in HSP90 Monitored Time Resolved and Label Free-Towards a Conformational Activity Screening for Drug Discovery., *Angew. Chem. Int. Ed.* **57**, 9955 (2018).
- <sup>25</sup>N. Michaud-Agrawal, E. J. Denning, T. B. Woolf, and O. Beckstein, Mdanalysis: A toolkit for the analysis of molecular dynamics simulations, *J. Comput. Chem.* **32**, 2319 (2011).
- <sup>26</sup>F. Sittel, A. Jain, and G. Stock, Principal component analysis of molecular dynamics: On the use of Cartesian vs. internal coordinates, *J. Chem. Phys.* **141**, 014111 (2014).
- <sup>27</sup>T. Kluyver et al., Jupyter Notebooks-a publishing format for reproducible computational workflows., in *Positioning and Power in Academic Publishing*, edited by F. Loizides and B. Schmidt, pages 87–90, IOP Press, 2016.
- <sup>28</sup>S. van der Walt, S. C. Colbert, and G. Varoquaux, The NumPy Array: A Structure for Efficient Numerical Computation, *Comput. Sci. Eng.* **13**, 22 (2011).
- <sup>29</sup>P. Virtanen et al., SciPy 1.0: fundamental algorithms for scientific computing in Python, *Nat. Methods* **17**, 261 (2020).
- <sup>30</sup>A. M. Price-Whelan, B. M. Sipcz, H. M. Gnther, P. L. Lim, S. M. Crawford, S. Conseil, D. L. Shupe, M. W. Craig, N. Dencheva, and et al., The astropy project: Building an open-science project and status of the v2.0 core package, *Astron. J.* **156**, 123 (2018).
- <sup>31</sup>J. D. Hunter, Matplotlib: A 2D graphics environment, *Comput. Sci. Eng.* **9**, 90 (2007).
- <sup>32</sup>Schr dinger, LLC, The PyMOL Molecular Graphics System, Version 1.8, (2010).
- <sup>33</sup>B. Efron and C. Stein, The Jackknife Estimate of Variance, *Ann. Stat.* **9**, 586 (1981).
- <sup>34</sup>E. S. Pearson, I. Note on Tests for Normality, *Biometrika* **22**, 423 (1931).
- <sup>35</sup>M. Amaral, D. B. Kokh, J. Bomke, A. Wegener, H. P. Buchstaller, H. M. Eggenweiler, P. Matias, C. Sirrenberg, R. C. Wade, and M. Frech, Protein conformational flexibility modulates kinetics and thermodynamics of drug binding., *Nat. Commun.* **8**, 2276 (2017).
- <sup>36</sup>R. Hall, T. Dixon, and A. Dickson, Correction Terms for Calculating Binding Free Energy Using Rates from Nonequilibrium Simulations, *ChemRxiv* (2020).
- <sup>37</sup>M. Post, S. Wolf, and G. Stock, Principal component analysis of nonequilibrium molecular dynamics simulations, *J. Chem. Phys.* **150**, 204110 (2019).
- <sup>38</sup>M. Ernst, F. Sittel, and G. Stock, Contact- and distance-based principal component analysis of protein dynamics, *J. Chem. Phys.* **143**, 244114 (2015).
- <sup>39</sup>S. Bray, *Approaches to analyzing protein-ligand dissociation with targeted molecular dynamics*, Master Thesis, 2018.
- <sup>40</sup>D. Bryant and V. Moulton, Neighbor-net: an agglomerative method for the construction of phylogenetic networks., *Mol. Biol. Evol.* **21**, 255 (2004).

- <sup>41</sup>R. O. Dror, A. C. Pan, D. H. Arlow, D. W. Borhani, P. Maragakis, Y. Shan, H. Xu, and D. E. Shaw, Pathway and mechanism of drug binding to G-protein-coupled receptors, *Proc. Natl. Acad. Sci. USA* **108**, 13118 (2011).
- <sup>42</sup>H. J. C. Berendsen, *Simulating the Physical World*, Cambridge University Press, Cambridge, 2007.
- <sup>43</sup>D. Nagel, A. Weber, B. Lickert, and G. Stock, Dynamical coring of Markov state models, *J. Chem. Phys.* **150**, 094111 (2019).
- <sup>44</sup>N. Schaudinnus, B. Lickert, M. Biswas, and G. Stock, Global Langevin model of multidimensional biomolecular dynamics, *J. Chem. Phys.* **145**, 184114 (2016).
- <sup>45</sup>J. O. Daldrop, B. G. Kowalik, and R. R. Netz, External potential modifies friction of molecular solutes in water, *Phys. Rev. X* **7**, 041065 (2017).
- <sup>46</sup>I. Hughes and T. Hase, *Measurements and Their Uncertainties*, A Practical Guide to Modern Error Analysis, Oxford University Press, 2010.